REFINED 3D STRUT-AND-TIE MODEL FOR ANALYSIS AND DESIGN OF FOUR-PILE CAPS

by Carlos Meléndez, Juan Sagaseta, Pedro F. Miguel Sosa, Luis Pallarés Rubio

Biography:

Carlos Meléndez received his PhD from Universitat Politècnica de València, Spain in 2017. His research interests include finite element modelling of reinforced concrete structures, strut-and-tie modelling and development of computer-aided tools.

Juan Sagaseta is a Senior Lecturer at University of Surrey, UK. He received his PhD from Imperial College London in 2008. His research interests include shear, punching, strut-and-tie modelling, analysis of structural concrete under accidental actions and progressive collapse.

Pedro F. Miguel Sosa is a Professor at Universitat Politècnica de València, Spain. He received his PhD in 1980. His research interests include strut-and-tie modelling, numerical and experimental analysis of concrete structures and shear.

Luis Pallarés Rubio is an Associate Professor at Universitat Politècnica de València, Spain. He received his PhD in 2006. His research interests include experimental and numerical analysis of structural concrete and masonry, and strut-and-tie modelling.

ABSTRACT

Pile caps used in foundations are commonly designed for simple cases of loading and geometry using the strut-and-tie method. This approach is known to provide safe designs and rather conservative predictions of the ultimate failure load of tests. This level of conservatism is due mainly to the large simplifications made in the geometry assumed which in many cases ignore relevant parameters such as the size of the column. A three-dimensional strut-and-tie

model is presented for four-pile caps in which the geometry adopted is optimized. The inclination of the direct strut from the column to the pile is obtained analytically through the maximization process of the resisting load carried by the truss assuming different modes of failure (flexural and shear). This approach is shown to provide more accurate predictions of strength of existing deep pile cap tests with lower scatter compared to design approaches in the literature and ACI 318 Code.

Keywords: pile cap, reinforced concrete, strut-and-tie method, truss model, design, discontinuity region, shear, three-dimensional, finite element analysis

INTRODUCTION

A pile cap is a foundation element commonly found in construction that is used to transfer loads from the superstructure to a group of piles. It often consists of a lightly reinforced concrete block with no shear reinforcement which is cast on top of the piles. The structural behavior of pile caps can be complex and several simplifications are generally made in design. Design procedures based on test results, rules of thumb and past experience were frequently followed in the past. A significant progress was made in the last decades with the proposal of more consistent design methods[1,2,3,4,5,6]. However, comparison of the predictions obtained by these methods shows a significant scatter in the results as shown in this paper. Of special concern is the fact that some of these methods can overestimate the shear strength, leading in some cases to brittle failures in elements designed to fail in a ductile flexural manner. This generally explains why simplifications and conservative assumptions are still common in design codes. Refinement of current analytical approaches could derive in more efficient designs which in turn will reduce material needs, construction times and costs.

Pile caps can be classified based on the shear span-to-depth ratio w/d as slender ($w/d>1$) or deep (thick) ($w/d<1$)[7]: the former behave governed by flexure and in the latter arching action

is the predominant resisting mechanism. This paper and previous experimental programs and design methods focus mainly on the latter case.

Deep pile caps are discontinuity regions (D-Regions), characterized by the development of complex stress fields. Two-way shear failures, with or without reinforcement yielding, of deep pile caps designed to fail in flexure are very common in the reported experimental campaigns[1,2,3,8,9,10,11]. This type of failure is characterized by the formation of a conical plug under the column or punching around one or more piles (Fig. 1).

Two different approaches are accepted for pile cap design in the ACI 318-14[12] and other major codes of practice. The traditional design procedure considered in the ACI Building Code is based on a sectional force approach. This approach seems adequate for slender pile caps, however it is contentious[3,4] whether it is also valid for deep pile caps as some of the main assumptions of sectional analysis do not apply (i.e. flexural compression is non-uniform along the cap width, plane sections do not remain plane and shear stresses are not uniform along the cap depth). Alternatively to sectional-based approaches, the strut-and-tie method[13] (STM) is also accepted by the ACI Building Code since the ACI 318-02. The STM is a lower-bound method which is especially appropriate for the design of D-Regions. The application of the method is conceptually simple: after adopting an idealized truss formed by concrete struts, steel ties and nodal zones, forces at the truss elements are obtained from equilibrium and compared with their corresponding estimated strengths to determine the maximum admissible load. The typical strut-and-tie model of a pile cap is formed by inclined struts expanding from the column to the piles and horizontal ties between the piles. Two- and three-dimensional models are generally considered (Fig. 2); 2D models are usually preferred in practice due to the lack of general guidelines for the application of the STM in 3D[14].

In the scientific literature for pile cap analysis and design, most analytical models proposed

are based on spatial 3D truss models[3,4,5,6,15,16,17,18]; some of these models are reviewed in this paper. Most of these references focus on the proposal of different formulae to estimate a concrete strength effectiveness factor in order to reproduce accurately the failure load, but little attention is paid on the truss geometry and a predefined truss geometry is generally assumed for simplicity. The use of more refined models derived by iteration of the truss geometry could lead to better initial predictions which would not need further adjusting[19].

This paper presents a new, alternative STM-based approach for the analysis and design of deep pile caps. A refined truss geometry is considered, with the strut inclination being determined by maximizing the pile cap strength considering different failure conditions. The method is developed for rectangular four-pile caps without shear reinforcement and concentrically loaded with a square column, a configuration which is commonly found in construction. The proposed model satisfies equilibrium, strain compatibility and considers softening of the compressive strength for cracked concrete. It also accounts for the effect of reinforcement area and configuration (distribution and anchorage conditions) to estimate the shear strength, factors which are not considered in previous models; this leads to a more precise prediction of the shear strength, hence reducing the potential of occurrence of brittle failures. For the validation of the proposed method, strength predictions obtained by the proposed and other five methods of 162 pile cap specimens are compared and discussed. The adequacy of the adopted model is further verified by means of 3D FE analysis.

RESEARCH SIGNIFICANCE

Four-pile caps are commonly used in practice and optimizing their design can result in substantial cost savings. Current design approaches can give significantly different results, which often leads to the adoption of excessively conservative solutions. This paper describes an alternative approach for the design of four-pile caps based on a refined three-dimensional

strut-and-tie model where the strut inclination is determined by maximizing the pile cap strength. The method considers strength softening of cracked concrete, compatibility constraints and reinforcement details. Consideration of this model could lead to a more rational design procedure of deep pile caps.

DESIGN METHODS FOR PILE CAPS

Existing truss-based models for pile cap design

Several strut-and-tie-based models have been proposed in the literature for pile cap design. Although the geometric shape of the truss models adopted by different authors is fundamentally similar, the location of the nodes, and hence the resulting strut inclination θ_s^{3d}, do not always coincide. Truss forces can be expressed as a function of θ_s^{3d} as (Fig. 2):

$$F_s = \frac{P}{4\sin\theta_s^{3d}} \qquad (1)$$

$$F_{t,x} = \frac{P\cos\varphi}{4\tan\theta_s^{3d}} = \frac{P}{4\tan\theta_{s,x}^{2d}} \qquad (2)$$

$$F_{t,y} = \frac{P\sin\varphi}{4\tan\theta_s^{3d}} = \frac{P}{4\tan\theta_{s,y}^{2d}} \qquad (3)$$

It should be noted that, despite the 3D geometry of the truss, resulting tie forces from Eq. (2) and (3) are equal to those obtained from a 2D model (Fig. 2(b)). Therefore 2D and 3D trusses will result in the same area of reinforcement if the design is merely based on tie forces.

The design method proposed by Blévot and Frémy[1] is one of the first references on pile cap analysis using truss models. For four-pile caps they adopted a truss model with four lower nodes located at the centre of the piles at the reinforcement level and four upper nodes at the column quarter points on the cap surface. Based on test results it was suggested to limit the steel stress to $0.6f_y$ and the bearing stress at the piles and the column to $0.9f_c^{'}\sin^2\theta_s^{3d}$.

Adebar et al.[3] studied the suitability of three-dimensional strut-and-tie models in pile cap design and adopted a truss model formed by four upper nodes considering the depth of the

compressive stress block under the column. To evaluate the flexural capacity the steel stress was limited to the yield stress f_y and to prevent shear failures the maximum bearing stress on concrete was limited to $f_c^{'}$. The latter limitation was later refined by Adebar and Zhou[4] as:

$$f_b \le 0.6 f_c^{'} + \alpha\beta 6\sqrt{f_c^{'}}$$
$$\alpha = 0.33\sqrt{(A_2 / A_1 - 1)} \le 1.0 \quad (4)$$
$$\beta = 0.33(h_s / w_s - 1) \le 1.0$$

where $f_c^{'}$ has units of MPa (if psi units are used, factor 6 in Eq. (4) must be replaced by 72). Factors α and β account for confinement according to the strut geometry (i.e. A_1 and A_2 are the loaded and supporting area respectively, and h_s / w_s is the strut height-to-width ratio). Otherwise, the adopted truss model was identical to that proposed by Blévot and Frémy.

Park et al.[5] developed a 3D strut-and-tie approach that considered strain compatibility, concrete compressive softening and a nonlinear constitutive relationship for concrete. Failure could be caused by crushing or splitting of the diagonal strut, crushing of the horizontal compression zone under the column or reinforcement yielding. The upper nodes of the truss model were located at the column quarter points at half depth of the compressive stress block.

The truss model proposed by Souza et al.[6] was formed by only one upper node located at the center of the column on the cap surface (Fig. 2(a)). This simplification implied a significant change in the strut inclination and, hence, the forces resulting in the truss system. To determine the pile cap flexural strength the following equation was proposed:

$$P = \frac{4\phi_y d A_{sT} f_y}{e} \quad (5)$$

where ϕ_y was a calibration factor (equal to 2.05) giving the lowest coefficient of variation of the predicted test data. To predict the shear strength the model by Siao[20] was adopted:

$$P = 2.08 c d f_c^{2/3} \quad (6)$$

Guo[16] developed a strut-and-tie-based method for evaluating punching strength of pile caps

with uniform grid reinforcement. The adopted truss model was formed by one upper central node at 0.1 times the effective depth from the cap surface and four lower nodes at the reinforcement level slightly displaced from the center of the piles. Alternatively to lower-bound truss models Jensen and Hoang[21] proposed an upper bound plasticity approach for pile cap analysis to complement strut-and-tie models. Three independent collapse mechanisms were considered: (i) punching, (ii) shear and (iii) flexural.

Sectional methods vs. STM in the ACI 318-14 Code

According to the current ACI 318-14[12], both the sectional approach and the STM are permitted for pile cap design. The sectional method is applied similarly to two-way slabs and footings. The flexural and shear strength are evaluated separately. The flexural strength is governed by the amount of longitudinal reinforcement and is obtained assuming that (a) plane sections remain plane and (b) the concrete compressive block extends to the entire pile cap width. The flexural critical section is located at the face of the column. The shear strength is governed by the cap depth and the concrete strength and is determined by the most restrictive condition considering one-way and two-way shear. For one- and two-way shear the critical sections are located at d and $d/2$ from the column face, respectively.

$$\text{One - way shear}: V_c = 0.17\lambda\sqrt{f_c'}\,b_w d \quad (7)$$

$$\text{Two - way shear}: V_c = 0.33\lambda\sqrt{f_c'}\,b_0 d \quad (8)$$

where f_c' has units of MPa (if psi is used, Eq. (7) and (8) must be multiplied by 12). According to ACI 318-14 the shear due to the pile reaction at the critical section around the column shall be accounted for as follows: (i) when the pile center is located $d_p/2$ or more inside the section, the reaction produces no shear, (ii) when the pile center is located $d_p/2$ or more outside the section, the entire pile reaction shall be considered; and (iii) for intermediate positions, the portion of the pile reaction is obtained from a linear interpolation. An upper

limit on the shear strength shall be considered[22], where the following limits are proposed:

$$\text{One - way shear}: V_c = \frac{d}{w}\left(3.5 - 2.5\frac{M_u}{V_u d}\right)\left(0.16\lambda\sqrt{f_c'} + 17\rho\frac{V_u d}{M_u}\right)b_w d \le 0.83\sqrt{f_c'}b_w d \quad (9)$$

$$\text{Two-way shear}: V_c = \frac{d}{w}\left(1+\frac{\mathrm{d}}{\mathrm{c}}\right)\frac{1}{6}\sqrt{f_c'}b_o d \le 2.67\sqrt{f_c'}b_o d \quad (10)$$

where b_o is the column perimeter and f_c' is in MPa (for psi, the relationships above should be multiplied by 12). Application of the STM must be in accordance with the general guidelines of the ACI Code 318-14[12]. The area of reinforcement is calculated from the tie forces and the factored yield strength. Concrete stresses are limited to enable yielding of the reinforcement prior to failure: the compressive stresses in the struts shall not exceed $0.51f_c'$ assuming that no confinement reinforcement is present; considering general guidelines for 2D elements (no provisions are given for 3D nodal zones), the concrete compressive stress in the nodal zone underneath the column and over the piles shall be limited to $0.85f_c'$ and $0.51f_c'$, respectively. ACI 318-02, ACI 318-08 and ACI 318-11 restricted the application of the STM only to pile caps in which the distance between pile and column axes was equal or less than two times the height of the cap. No reference to limits of application is made in the current ACI 318-14.

PROPOSED STRUT-AND-TIE MODEL

Equilibrium in the three-dimensional model

A statically determinate 3D truss model was adopted to represent the load transmission from the column to the piles (Fig. 3). The position of the four lower nodes was fixed at the center of the piles at the reinforcement level and the upper nodes were located inside the column and above the cap surface. Unlike other truss-based models, the horizontal position of the top nodes was not assumed beforehand as the strut inclination θ_s^{3d} is a geometrical variable which will be obtained by maximizing the strength given by a lower-bound strength function derived as described later. Forces at diagonal struts and horizontal ties can be calculated from

equilibrium (Eq. (1-3)). The formulae presented hereafter were derived for a square-shape cap (e_x=e_y=e) loaded by a square column (c_x=c_y=c), which applies to most four-pile caps in practice. Hence, considering symmetry Eq. (2) and (3) can be merged into one as:

$$F_t = F_{t,x} = F_{t,y} = \frac{P}{4\tan\theta_s^{2d}} = \frac{P}{4\sqrt{2}\tan\theta_s^{3d}} \quad (11)$$

Considered local failure modes and corresponding limit functions

Three potential local failure modes were considered: mode (i) accounts for exceeding the reinforcement strength; mode (ii) accounts for crushing of the diagonal strut at the base of the column with narrowing of the strut; and mode (iii) accounts for splitting of the diagonal strut due to transverse cracking. The maximum admissible load was obtained for each local failure mode in terms of the variable strut angle θ_s^{3d}, pile cap geometry and material properties. This relationship is denoted as limit function for a local failure mode.

Mode (i)

In design, the limit function corresponding to yielding of the reinforcement was obtained by fixing the value of the tie force to its yield strength. Considering that reinforcement is distributed symmetrically in each horizontal direction, the latter can be calculated as:

$$F_{nt,y} = A_{ts} f_y = \frac{A_{sT}}{2} f_y \quad (12)$$

where A_{sT} is the total amount of reinforcement in the considered direction (Fig. 3(d)). The maximum column load limited by reinforcement yielding (limit function associated to mode (i)) can be derived by equating Eq. (11) and Eq. (12) and is given by:

$$P_{nt,y} = 4\sqrt{2}\tan\theta_s^{3d} F_{nt,y} = 2\sqrt{2}\tan\theta_s^{3d} A_{sT} f_y \quad (13)$$

The analysis of 162 pile cap specimens from the literature, which are further described in subsequent sections, showed that specimens where $P_{nt,y}$ governed the failure load had a significant strength enhancement due to strain-hardening effects. For such cases of

assessment, a better prediction of the failure load was obtained by adopting the steel ultimate stress f_u rather than the yield stress f_y; i.e. $P_{nt,y}$ is replaced by $P_{nt,u}$ given by:

$$P_{nt,u} = 2\sqrt{2}\tan\theta_s^{3d} A_{sT} f_u \quad (14)$$

Eq.(14) considers strain-hardening of steel indirectly, leading to a further realignment of the strut after steel yielding providing more accurate predictions of the experimental data. This simplified approach was preferred over more complex solutions considering the plastic strains in the steel explicitly. Further implications and verification of this simplification for tests where $P_{nt,u}$ governed the failure load are discussed in subsequent sections.

Mode (ii)

Crushing of the diagonal strut was considered by limiting the force in the strut to its capacity at the top section where it narrows at the intersection between the pile cap and the column. This top region was not considered as a node, but rather as a critical region to assess the strut capacity. The maximum admissible load of the pile cap reduces as the strut inclination increases since the strut becomes narrower. The strut strength can be obtained as (Fig. 3):

$$F_{ns,1} = A_{cs,1} f_{cp} \quad (15)$$

$$A_{cs,1} = \frac{1}{2} w_{s,1} b_1 \quad (16)$$

$$w_{s,1} = l_t \frac{\sqrt{2}}{2}\sin\theta_s^{3d} = 3\left(\frac{d}{\sqrt{2}\tan\theta_s^{3d}} - w\right)\frac{\sqrt{2}}{2}\sin\theta_s^{3d} \quad (17)$$

$$b_1 = l_t\sqrt{2} = 3\left(\frac{d}{\sqrt{2}\tan\theta_s^{3d}} - w\right)\sqrt{2} \quad (18)$$

$$\begin{aligned} f_{cp} &= f_c^{'} \text{ if } f_c^{'} \le 20\text{MPa}(2900\text{psi}) \\ f_{cp} &= 2.7 f_c^{'2/3} \text{ if } f_c^{'} > 20\text{MPa (2900psi)} \end{aligned} \quad (19)$$

where $w_{s,1}$ is the strut width at the top section. The compressive strength of concrete was taken as the plastic strength f_{cp}[23], assuming an uncracked uniaxial compressive state. This

assumption was justified based on experimental observations showing that this region remains uncracked until failure and was further verified using 3D FE analysis as shown later. The strut area $A_{cs,1}$ was obtained from the projection of a horizontal triangle expanding from the column corner onto a plane perpendicular to the strut (Fig. 3(c)) where the stresses are constant. Considering Eq. (15-19) the nominal strength of the top section of the strut is

$$F_{ns,1} = 4.5\left(\frac{d}{\sqrt{2}\tan\theta_s^{3d}} - w\right)^2 \sin\theta_s^{3d} f_{cp} \quad (20)$$

Hence, the maximum admissible vertical load limited by crushing of the diagonal strut at its top section is obtained from Eq. (1) and Eq. (20) giving:

$$P_{ns,1} = 4\sin\theta_s^{3d} F_{ns,1} = 18 f_{cp}\left(\frac{d}{\sqrt{2}\tan\theta_s^{3d}} - w\right)^2 \sin^2\theta_s^{3d} \quad (21)$$

Mode (iii)

Splitting of the diagonal strut was considered by limiting the force in the strut to its capacity at the bottom where the strut meets the flexural reinforcement. The nominal splitting strength of the strut can be estimated as (Fig. 3):

$$F_{ns,2} = A_{cs,2} f_{ce} = A_{cs,2}\xi f_{cp} \quad (22)$$

$$A_{cs,2} = \beta_p w_{s,2} l_p \quad (23)$$

$$w_{s,2} = l_p \sin\theta_s^{3d} + 2c_b \cos\theta_s^{3d} \quad (24)$$

$$c_b = h - d \quad (25)$$

where $w_{s,2}$ is the strut width at the bottom. The concrete softening coefficient ξ is a strength reduction factor due to transverse strains. The model by Vecchio and Collins[24] was adopted:

$$f_{ce} = \xi f_{cp} = \frac{f_{cp}}{0.8 + 170\varepsilon_{st}} \le f_{cp} \quad (26)$$

where ε_{st} is the tensile strain transverse to the principal compressive direction. To extend this

relationship to 3D, it was assumed that the two principal strains perpendicular to the strut $\varepsilon_{st,1}$, $\varepsilon_{st,2}$ contribute equally to softening and ε_{st} in Eq. (26) was replaced by $\varepsilon_{st,1}+\varepsilon_{st,2}$. This sum can be obtained from the first invariant of the strain tensor and considering perfect bond between concrete and steel as:

$$\varepsilon_x+\varepsilon_y+\varepsilon_z=\varepsilon_{tx}+\varepsilon_{ty}+\varepsilon_z=\varepsilon_{st,1}+\varepsilon_{st,2}+\varepsilon_s \quad (27)$$

Eq. (27) introduces a strain compatibility condition. The average compressive strain in the z-direction ε_z and the average compressive strain of the strut ε_s are estimated as:

$$\varepsilon_z=\frac{-P/4}{E_c A_p} \quad (28)$$

$$\varepsilon_s=\frac{-F_s}{E_c A_{cs,2}}=\frac{-P}{4\sin\theta_s^{3d} E_c A_{cs,2}} \quad (29)$$

The average tensile strain in the x- direction can be estimated from the steel strain as:

$$\varepsilon_{tx}=\frac{F_t}{E_s A_{sp,x}}=\frac{P}{4\tan\theta_s^{2d} E_s A_{sp,x}}=\frac{P}{4\sqrt{2}\tan\theta_s^{3d} E_s A_{sp,x}} \quad (30)$$

and ε_{ty} can be obtained similarly replacing $A_{sp,x}$ by $A_{sp,y}$. Eq. (30) is valid for cases where the reinforcement does not yield at failure; if this is not the case, this expression is an approximation where the strains are generally underestimated and hence the effective strength in the strut could potentially be overestimated. This could occur when adopting f_u as the steel stress limit in assessment (Eq. 14). However, the results presented in the next section show that this simplification gives reasonable strength predictions of the experimental data available. Adopting a more realistic relationship taking into account strain-hardening of the tie would introduce complexity with little improvement in accuracy in this case. In addition, the use of a more refined post-yielding relationship would be cumbersome as it would require introducing post-yielding properties for steel which are often not available in test reports.

In Eq. (30), the area of reinforcement over the pile $A_{sp,j}$ for each direction j, can be written as a fraction of the total reinforcement area $A_{sT,j}$: for bunched reinforcement in symmetrical cases, $A_{sp,j}$ is taken as half $A_{sT,j}$, assuming that all rebars are placed over the piles; for grid layouts with hook and nil anchorages (straight bars without hooks), $A_{sp,j}$ can be calculated as:

$$\begin{aligned} A_{sp,j} &= A_{sT,j}\frac{d_p + c_b}{e + d_p} \quad \text{for circular piles} \\ A_{sp,j} &= A_{sT,j}\frac{l_j + c_b}{e + l_j} \quad \text{for square and rectangular piles} \end{aligned} \qquad (31)$$

assuming that rebars are distributed uniformly between the outside edges of the piles and considering the spread of the diagonal strut at the reinforcement level; and for grid layouts with full anchorage, $A_{sp,j}$ is taken equal to $A_{sT,j}/2$ to consider confinement effects.

$A_{cs,2}$ is obtained by projecting the pile section onto a plane perpendicular to the inclined strut passing through the lower node of the strut as shown in Fig. 3(c). If the pile section is circular, the projection is an ellipse with minor and major axis equal to l_p and $w_{s,2}$ respectively (i.e. $\beta_p = \pi/4$ and l_p is the diameter of the pile d_p). If the pile section is rectangular, the projection is a rhombus with l_p and $w_{s,2}$ diagonals (i.e. $\beta_p = 0.5$ and l_p is the diagonal of the pile section). For pile caps with $e/d > 2$, where the behavior is closer to a beam factor β_p is taken equal to 1 (rectangular projection) for both circular and square piles.

The maximum admissible vertical load limited by splitting of the diagonal strut (limit function associated to local failure mode (iii)) is obtained from Eq. (1) and Eq. (22-31):

$$P_{ns,2} = 4\sin\theta_s^{3d} F_{ns,2} = \frac{4\beta_p \sin\theta_s^{3d}\left(l_p \sin\theta_s^{3d} + 2c_b\cos\theta_s^{3d}\right) l_p f_{cp}}{0.8 + 170\left(\varepsilon_{tx} + \varepsilon_{ty} + \varepsilon_z - \varepsilon_s\right)} \qquad (32)$$

Evaluation of the strength and the global mode of failure

The lower-bound strength function of the element P_n can be defined by the three limit functions ($P_{nt,u}$, $P_{ns,1}$, $P_{ns,2}$) given by Eq. (14), Eq. (21) and Eq. (32) as:

$$P_n = \min\left(P_{nt,u}, P_{ns,1}, P_{ns,2}\right) \quad (33)$$

This function, which varies with θ_s^{3d} , defines an area below of admissible loads and strut angles (Fig. 4) in which equilibrium is achieved without failure (lower-bound theorem of plasticity). Therefore, the best estimation of the pile cap strength P_{pred} will be the maximum (peak) value of the lower-bound strength function P_n in Eq. (33). The peak point P_{pred} and its corresponding strut inclination θ_{pred}^{3d} can be obtained from the intersection between $P_{ns,1}$ and $P_{ns,2}$ or between $P_{ns,1}$ and $P_{nt,u}$, whichever gives the lowest load. The intersection between $P_{ns,1}$ and $P_{ns,2}$ represents the shear strength P_s whereas the intersection between $P_{ns,1}$ and $P_{nt,u}$ represents the flexural strength P_f as shown in Fig. 4. Therefore, the predicted global mode of failure can be assessed based on which intersection point governs (Fig. 4). Shear failure can take place prior reinforcement yielding (Fig. 4(b)) when $P_s < P_{nt,y}$ for $\theta_s^{3d} = \theta_{pred}^{3d}$ or after yielding (Fig. 4(c)) when $P_s > P_{nt,y}$ for $\theta_s^{3d} = \theta_{pred}^{3d}$.

Finding the predicted strength and mode of failure using the proposed model can be done by hand or numerically using a simple spreadsheet. Eq. (32) for $P_{ns,2}$ is implicit; strains ε_{tx} , ε_{ty} , ε_z and ε_s are a function of the column load P , which is unknown a priori. To simplify the solution procedure it is suggested to assign an initial value P_{est} to estimate strains in Eq. (28-30). A good initial value is P_f , which is obtained independently of $P_{ns,2}$. P_{est} can be updated in later steps of the iterative process by P_s until convergence is achieved.

Relevance of the proposed method

Existing strut-and-tie models for pile caps evaluate separately the flexural and the shear strength with two independent equations and the strut inclination is fixed by the geometry. The model presented here considers that the strut inclination is unknown a priori. As one additional variable was included, one extra equation was needed. Limit function $P_{ns,1}$ (Eq. 21) was added to the usual equations to determine both the flexural and the shear strength. This function considers the realignment of the strut to steeper angles while cracking which allows stress redistribution and the application of further load increments. This realignment is possible due to stress redistribution within the stub column. The proposed model accounts for the reinforcement area and its layout to determine the shear strength of pile caps. These two factors, which are not considered in existing models except in reference[21], have been shown to have an effect on the shear strength: an increase of the reinforcement quantity[6] or its concentration over the piles leads to higher shear strengths[1,2,3,8]. In the proposed model the reinforcement area and its layout influence the strut strength through the effective concrete compressive strength f_{ce}; this in turn influences the pile cap strength. Only the reinforcement over the piles A_{sp}, which is assumed to contribute to resist the tensile stresses, is considered. Hence, the estimated steel tensile strains are lower for bunched configurations than for grid layouts with the same total amount of reinforcement; this assumption is consistent with experimental observations reporting higher failure loads for configurations with concentrated reinforcement[1,2,3,8].

VALIDATION WITH TEST RESULTS

The proposed model was validated against 162 pile cap tests reported in the literature[1,2,8,9,10,11,25] (Table 1). All specimens had a square shape in plan, had no shear reinforcement and were loaded at a centered square column. The proposed approach was

applied assuming that the reinforcement is placed along the sides of the cap. Tie areas of specimens with diagonal reinforcement were calculated by projecting the tie forces onto the x- and y-axis. For all specimens, the elastic moduli adopted for steel and concrete were 200000 MPa (29000 ksi) and $4750\sqrt{f_c'}$ (MPa) ($57000\sqrt{f_c'}$ (psi))[12].

Table 1 shows the ratio between the maximum load in the test and the predicted strength (P_{test}/P_{pred}) and the predicted global mode of failure. The average value of P_{test}/P_{pred} for the 162 tests is 1.08 with coefficient of variation equal to 12%. Comparison of the predicted and observed modes of failure shows a correct estimation in 55% of the cases. This seems reasonable considering firstly, the uncertainty in identifying the mode of failure from test data as the failure of many of the specimens may be more accurately described as a combination of bending and shear; and secondly, the fact that the predicted shear and flexural strengths were very close to each other in many tests as shown in the last column in Table 1. If shear failure with and without yielding of the reinforcement are considered as one mode of failure, then the predicted and observed failure modes coincide in 75% of the cases. It can be concluded that the model predicts the strength and mode of failure with reasonable accuracy.

VERIFICATION WITH FE RESULTS

The assumptions made in the proposed method were further verified by means of FE analysis obtained with the 3D nonlinear FE-based tool FESCA 3D[26], developed at Universitat Politècnica de València. The FE tool had been validated beforehand for the analysis of reinforced concrete pile caps as shown in[26]. This tool was used to visualize the internal stress flow and to obtain the concrete strength reduction field within the pile cap $\xi(x, y, z)$ in order to compare it with the values adopted and estimated in the proposed model.

The main characteristics of the constitutive material model used in the numerical tool are described in[26]. The following assumptions were adopted to verify the adequacy of the

proposed model. The concrete in tension was modelled using Hordijk's softening curve after cracking with the tensile strength given by $f_{ct} = 0.21 f_c'^{2/3}$ (MPa units) and the fracture energy $G_f = 73 f_c'^{0.18}$ (N/m and MPa units, respectively) as defined in MC 2010[27]. The concrete in compression was modelled using a parabolic relationship; compressive softening due to transverse tensile strains was considered adopting the relationship proposed in[24] (Eq. (26)); enhancement of the compressive strength of concrete due to confinement was taken into account using a Drucker-Prager yield surface. Reinforcement steel was modelled as an elastic-hardening plastic material assuming perfect bond between the concrete and the steel.

Fig. 5 shows the FE results obtained for specimen BP-30-30-2 from reference[8] which failed in shear after reinforcement yielding. The load-deflection response was predicted accurately as shown in Fig. 5(a). Fig. 5(b) and (c) show the principal compressive stress field and trajectories in the cap diagonal plane at maximum load and after failure respectively. The proposed strut-and-tie model resulted in a strut inclination of $\theta_{pred}^{3d} = 48.64º$. This angle and the associated strut widths are consistent with the FE compressive stress field (Fig. 5(b-c)).

Fig. 5(d-e) show the FE contour plot of the concrete softening coefficient ξ obtained in the diagonal plane of the cap at the maximum load and immediately afterwards. The proposed method adopts ξ equal to 1 at the top region of the strut whereas at the bottom Eq. (26) gave a value of 0.5 in this case; these results are consistent with FE predictions shown in Fig. 5(e).

Regarding failure, the numerical model predicts that strut softening initiates at the bottom due to steel yielding and propagates to the top (Fig. 5(d-e)); this weakening of the strut results in a stress redistribution with a realignment of the strut which becomes steeper and narrower in the region near the column. This behavior is consistent with the predicted mode of failure using the limit functions proposed in this work and observed in the deep pile cap test.

COMPARISON WITH EXISTING METHODS

Five of the existing lower-bound methods described in this paper (ACI sectional force and STM approach[12], Adebar and Zhou[4], Souza et al.[6] and Park et al.[5]) were applied to predict the failure load of the 162 specimens investigated (Fig. 6). The accuracy of the predictions was expected to vary from one method to another as the design philosophy and complexity behind each approach is considerably different. For example, the ACI STM approach, whilst simple, is expected to provide a lower-bound solution with no focus on the scatter of the results.

Provisions for shear design with the ACI sectional approach[12], considering the stress limits from the CRSI Handbook[22], lead to unconservative shear strength predictions of many of the pile caps investigated (Fig. 6(a)). The majority of the specimens are predicted to fail in flexure whereas in reality many tests failed in shear. On the other hand, the ACI STM approach[12] provide conservative predictions of all the tests (Fig. 6(b)). The high level of conservatism in some cases can be questioned due to its economic implications in design.

Predictions by the approach by Adebar and Zhou[4] (Fig. 6(c)) have a relatively low scatter ($COV = 21\%$) although most failures are predicted incorrectly as flexural. The proposed bearing stress limit governs in 17 out of 162 specimens. For these 17 specimens the average strength ratio P_{test} / P_{pred} is 1.03, with a coefficient of variation of 20%; these results are remarkable considering the simplicity of the method. Predictions by the model by Souza et al.[6] (Fig. 6(d)) also have a low scatter ($COV = 23\%$) with an average value of the P_{test} / P_{pred} ratio of 1.01. It should be noted that the formula proposed for estimating the flexural strength was calibrated with experimental results, most of which were included in the current study. The shear design formula by Souza et al. does not capture correctly the influence of the pile cap depth on the shear strength similarly to the ACI sectional approach; both approaches overestimate the shear strength because they assume that the whole depth contributes to resist

the transverse tensile stresses. However, the internal flow of forces in the pile cap exhibits stress concentration at certain areas of the section as shown in FE analysis (Fig. 5); this is correctly identified in the proposed strut-and-tie model (only limited areas of the concrete section contribute to resist the shear stresses). The model proposed by Park et al.[5] provides predictions on the conservative side (Fig. 6(e)). The shear strength is clearly underestimated, resulting in large P_{test}/P_{pred} ratios in some of the specimens.

The proposed approach has the lowest coefficient of variation (12%) with an average value slightly above one (1.08) (Fig. 6(f)). The refinement of the strut-and-tie geometry and the consideration of reinforcement area and layout in the determination of the effective strut strength are behind the accuracy in the strength predictions. Related to the former, in Fig. 7(a) the strut inclinations obtained analytically for each specimen with the proposed model θ_{pred}^{3d} are compared with those obtained assuming a fixed strut inclination θ_{o}^{3d} with the upper nodes located at quarter points at the column. It is worth noting that a 5º difference can result in a variation of the tie forces of around 20% and in the strut forces between 5-20%, depending on the strut inclination. These angle differences can be even larger if the strut inclination is fixed using an upper central node[6,16] or if upper nodes are located below the top of the cap[5,28].

Regarding the effect of the reinforcement area, Fig. 7(b) shows the strength predicted by the proposed model for different reinforcement quantities A_{sT} and shear span-to-depth ratios w/d of a symmetric four-pile cap with circular piles of diameter 150mm, c=250mm, d=300mm, f_c'=30MPa and grid reinforcement with f_y=356MPa and f_u=501MPa (larger strengths are obtained with bunched reinforcement). Predictions from the STM approach of the ACI Code and experimental data from twelve specimens TDL1-1/2, TDL2-1/2, TDL3-1/2, TDS1-1/2, TDS2-1/2 and TDS3-1/2 reported in reference[9] and with similar characteristics are added for comparison in Fig. 7(b). The curves in Fig. 7(b) show two distinctive regions: flexural failure

governs in the first section and shear failure governs in the second one. The amount of reinforcement increases the predicted strength in both ranges, but this effect is significantly lower when shear failure governs. Fig. 7(b) also shows that the reduction of the predicted strength with *w/d* is nonlinear.

DESIGN APPROACH PROPOSED

A design approach is presented based on the refined 3D strut-and-tie model developed herein (Fig. 8); this approach can be used easily to obtain the area of flexural reinforcement needed and check the adequacy of the cap geometry for a given design load P_u. For design, the steel yield stress f_y shall be used. The strut angle θ_u^{3d} is determined by taking $P_{ns,1} = P_u$ (Eq. (21)) and the reinforcement area A_{sT} can be obtained introducing θ_u^{3d} in Eq. (13) and considering $P_{mt,y} = P_u$. To ensure reinforcement yielding prior shear failure P_u must be lower than the maximum admissible value $P_{ns,2}$ (Eq. (32)) at the angle obtained previously θ_u^{3d}. If this condition is not fulfilled, the geometry of the pile cap should be modified (e.g. increase the cap depth). Simplified expressions are given in Fig. 8 to apply this procedure.

Overall, the proposed design approach seems more rational than existing methods as it takes into account three local failure modes, giving accurate strength predictions with significantly reduced scatter. Moreover, the proposed method gives a geometry of the strut-and-tie model following a rational approach rather than adopting a simplified geometry. Hence, this approach could provide more economic and consistent designs than existing methods.

SUMMARY AND CONCLUSIONS

Design of deep pile caps can be problematic in some cases where overly simplified models are extrapolated to complex situations. Traditionally, empirical approaches, rules of thumb and sectional-based methods were used. The STM emerged as a more consistent and rational

alternative and today most major codes of practice, including ACI 318-14[12], accept its application. However, a look at design codes and current practice shows that sectional methods still prevail in the design of deep pile caps, probably due to the limited guidelines on 3D STM and also on the misperception that lower-bound methods are too conservative.

This paper describes a 3D strut-and-tie-based model for the analysis and design of deep four-pile caps without shear reinforcement. One of the main innovations of this model is the use of a variable strut angle; existing models assume a fixed inclination of the strut. The proposed approach also gives information on the predominant mode of failure which is consistent with observation from tests and 3D FE simulations. Three potential local failure modes were considered: (i) exceeding the reinforcement strength, (ii) crushing of the strut at the base of the column and (iii) splitting of the strut near the pile; then three limit functions were defined, from which the predicted failure load and strut angle at failure can be determined.

The model takes into account the refined inclination of the strut, the effect of the reinforcement area and the type of reinforcement layout. These refined considerations resulted into very good strength predictions of the 162 tests investigated. The proposed model had the lowest coefficient of variation from all the methods investigated (*COV*=12%) with an average P_{test} / P_{pred} ratio of 1.08. It can be concluded that equilibrium models using struts with refined values of their inclination and concrete effective strength (based on strains) can provide economic designs and accurate predictions of pile cap strength.

ACKNOWLEDGMENTS

The authors wish to thank the Spanish Ministry of Education for the FPU fellowship FPU12-01459 received by the first author and the funding provided for his research stay at University of Surrey. The authors also wish to thank the Spanish Ministry of Economy and Competitiveness. for funding Project BIA 2012-32300.

NOTATION

b_w = pile cap width

b_o = perimeter of critical section for two-way shear

b_1, l_t = dimensions of the stressed triangle at the column base

c_x , c_y = column dimensions in x and y direction, respectively (if symmetry, $c=c_x=c_y$)

c_b = distance from centroid of reinforcement to nearest concrete surface

d = effective depth

d_p = pile diameter

e_x , e_y = pitch between center of piles in x and y direction (if symmetry, $e=e_x=e_y$)

f_c' = cylinder compressive strength of concrete

f_{ce} = effective compressive strength of concrete in a strut

f_{cp} = equivalent plastic strength of concrete

f_u , f_y = steel ultimate and yield stress, respectively

h = height of pile cap

h_s = length of strut as defined in reference[4]

l_p = diameter or diagonal of the pile

l_x , l_y = side lengths of rectangular pile

w = shear span defined as horizontal distance from face of column to center of pile reaction

w_s = strut width

A_1, A_2 = loaded and supporting surface area for consideration of bearing strength, respectively

A_p = pile sectional area

A_{sT} = total amount of horizontal reinforcement in one direction

A_{cs} = cross-sectional area of a strut, taken perpendicular to the axis of the strut

A_{sp} = area of reinforcement over pile in one direction

A_{ts} = area of non-prestressed reinforcement of a tie

F_{ns}, F_{nt} = nominal strength of a strut and a tie, respectively

F_s, F_s' = force in a strut in 3D and projected in 2D, respectively

F_{tx}, F_{ty} = force in a tie in x and y direction, respectively (if symmetry, F_{tx}=F_{ty}=F_t)

M_u = factored moment at section

P, P_u = axial load applied in the column and column design load respectively

P_n = lower-bound strength function of the element

P_f, P_s = predicted flexural and shear strength of pile cap, respectively

P_{est} = estimated column load used in the iterative process to determine shear strength

P_{pred}, P_{test} = predicted and experimental pile cap strength respectively

$P_{nt,u}$, $P_{ns,1}$, $P_{ns,2}$, $P_{nt,y}$ = limit functions for local failure modes (i), (ii), (iii), and steel yielding.

V_c = nominal shear strength provided by concrete

V_u = factored shear force at section

α, β = parameters used by Adebar et al.[4] (Eq. 4)

β_p = area factor of the projection of the pile perpendicular to the strut direction

ε_{st}, $\varepsilon_{st,1}$, $\varepsilon_{st,2}$ = average principal tensile strain in concrete

ε_s = average compressive strain of the concrete strut

ε_x, ε_y, ε_z = average concrete strain in x, y and z direction

ε_{tx}, ε_{ty} = reinforcement strain in x and y direction

λ, ν_u = slenderness and load parameters used in the design approach proposed

θ_{pred}^{3d}, θ_{u}^{3d} = predicted strut inclination at failure and resulting strut inclination in design

$\theta_{s,x}^{2d}$, $\theta_{s,y}^{2d}$ = strut angle projection in 2D at y=const and x=const, respectively

θ_{s}^{3d} = 3D strut angle

φ = angle between the tie in the x-direction and the horizontal projection of the diagonal strut

ξ = softening coefficient for cracked concrete strength

ϕ_{y} = calibration factor used by Souza et al.[6]

REFERENCES

1. Blévot JL, Frémy R. Semelles sur Pieux. *Inst Tech du Batim des Trav Publics*. 1967;20(230):223-295.
2. Clarke JL. *Behaviour and Design of Pile Caps with Four Piles*. Cement and Concrete Association. 1973; Report 42.489, London.
3. Adebar P, Kuchma D, Collins MP. Strut-and-Tie Models for the Design of Pile Caps: An Experimental Study. *ACI Struct J*. 1990;87(1):81-92.
4. Adebar P, Zhou L. Design of Deep Pile Caps by Strut-and-Tie Models. *ACI Struct J*. 1996;93(4):1-12.
5. Park J, Kuchma D, Souza R. Strength predictions of pile caps by a strut-and-tie model approach. *Can J Civ Eng*. 2008;35:1399-1413.
6. Souza R, Kuchma D, Park J, Bittencourt T. Adaptable Strut-and-Tie Model for Design and Verification of Four-Pile Caps. *ACI Struct J*. 2009;106(2):142-150.
7. Gogate AB, Sabnis GM. Design of Thick Pile Caps. *ACI J*. 1980;77(1):18-22.
8. Suzuki K, Otsuki K, Tsubata T. Influence of Bar Arrangement on Ultimate Strength of Four-Pile Caps. *Trans Japan Concr Inst*. 1998;20:195-202.
9. Suzuki K, Otsuki K, Tsubata T. Experimental Study on Four-Pile Caps with Taper. *Trans Japan Concr Inst*. 1999;21:327-334.
10. Suzuki K, Otsuki K, Tsuchiya T. Influence of Edge Distance on Failure Mechanism of Pile Caps. *Trans Japan Concr Inst*. 2000;22:361-368.
11. Suzuki K, Otsuki K. Experimental Study on Corner Shear Failure of Pile Caps. *Trans Japan Concr Inst*. 2002;23:303-310.
12. ACI Committee 318. *Building Code Requirements for Structural Concrete (ACI 318-14) and Commentary (ACI 318R-14).* American Concrete Institute; 2014.

13. Schlaich J, Schafer K, Jennewein M. Toward a Consistent Design of Structural Concrete. *PCI J*. 1987;32(May-June):74-150. doi:10.15554/pcij.05011987.74.150
14. Reineck K, Lourenço MS, Almeida JF, Haugerud S. Gaining Experience with Strut and Tie Models for the Design of Concrete Structures. In: *Design Examples for Strut-and-Tie Models, Fib Bulletin 61*. ; 2011:197-216.
15. Bloodworth AG, Cao J, Xu M. Numerical Modeling of Shear Behavior of Reinforced Concrete Pile Caps. *J Struct Eng*. 2012;138(6):708-717.
16. Guo H. Evaluation of Column Load for Generally Uniform Grid-Reinforced Pile Cap Failing in Punching. *ACI Struct J*. 2015;112(2):123-134.
17. Yun YM, Kim B, Ramirez JA. Three-Dimensional Grid Strut-and-Tie Model Approach in Structural Concrete Design. *ACI Struct J*. 2018;115(1):15-25.
18. Miguel-Tortola L, Pallarés L, Miguel PF. Punching shear failure in three-pile caps: Influence of the shear span-depth ratio and secondary reinforcement. *Eng Struct*. 2018;155:127-143. doi:10.1016/j.engstruct.2017.10.077
19. Sagaseta J, Vollum RL. Shear design of short-span beams. *Mag Concr Res*. 2010;62(4):267-282. doi:10.1680/macr.2010.62.4.267
20. Siao W Bin. Strut-and-Tie Model for Shear Behavior in Deep Beams and Pile Caps Failing in Diagonal Splitting. *ACI Struct J*. 1993;90(4):356-363.
21. Jensen UG, Hoang LC. Collapse mechanisms and strength prediction of reinforced concrete pile caps. *Eng Struct*. 2012;35:203-214. doi:10.1016/j.engstruct.2011.11.006
22. Concrete Reinforcing Steel Institute. *CRSI Handbook*. Schaumburg, Illinois; 2008.
23. Muttoni A, Schwartz J, Thürlimann B. *Design of Concrete Structures with Stress Fields*. Birkhäuser Verlag; 1997.
24. Vecchio FJ, Collins MP. The Modified Compression-Field Theory for Reinforced Concrete Elements Subjected to Shear. *ACI J Proc*. 1986;83(2):219-231.
25. Chan TK, Poh CK. Behaviour of precast reinforced concrete pile caps. *Constr Build Mater*. 2000;14:73-78.
26. Meléndez C, Miguel PF, Pallarés L. A simplified approach for the ultimate limit state analysis of three-dimensional reinforced concrete elements. *Eng Struct*. 2016;123:330-340. doi:10.1016/j.engstruct.2016.05.039
27. Fédération Internationale du Béton. *Model Code 2010*. Laussanne; 2013.
28. Comisión Permanente del Hormigón. *EHE-2008. Instrucción de Hormigón Estructural*. (Ministerio de Fomento). Madrid, Spain; 2008.

List of Tables:

Table 1 – Experimental data and predictions

List of Figures:

Table 1–Experimental data and predictions

Specimen	$f'_c \mid f_y \mid f_u$ (MPa)	$h \mid d \mid e \mid c \mid d_p$ (mm)	A_{sT}(mm^2) | Arrangmt., Anch. cond.	P_{test} (kN) | Fail. mode	P_{test}/P_{pred} | Fail. mode	$P_{s,pred}/P_{f,pred}$
Blévot and Frémy[1]						
4N1	37.3|277|401	750|675|1200|500|350(□)	7843|B,hook	7000|y+s	1.07|y+s	0.82
4N1bis	40.8|455|774	750|682|1200|500|350(□)	4824|B,hook	6700|s	1.11|y+s	0.64
4N2	37.1|285|416	750|660|1200|500|350(□)	7602|B+D,hook	6580|s	1.00|y+s	0.84
4N2bis	34.2|491|803	750|670|1200|500|350(□)	4816|B+D,hook	7390|s	1.32|s	0.60
4N3	34.2|257|387	1000|926|1200|500|350(□)	6085|B,hook	6500|f	0.85|y+s	0.90
4N3bis	49.3|452|781	1000|931|1200|500|350(□)	3941|B,hook	9000|y+s	1.12|y+s	0.72
4N4	35.4|291|413	1000|919|1200|500|350(□)	6702|B+D,hook	7530|y+s	0.94|y+s	0.83
4N4bis	42.3|486|811	1000|926|1200|500|350(□)	4384|B+D,hook	8750|s	1.13|s	0.63
2,2	32.8|355|428	300|277|420|150|140(□)	639|D,hook	810|f	1.02|f	1.06
2,3	31.6|312|409	300|259|420|150|140(□)	636|B+D,hook	740|y+s	1.04|f	1.18
2,4	31.0|330|425	300|261|420|150|140(□)	628|C,hook	705|f	0.97|f	1.14
3,1	32.1|469|643	200|180|420|150|140(□)	402|B,hook	475|y+s	0.98|f	1.37
3,2	37.2|447|589	200|177|420|150|140(□)	444|D,hook	540|f	1.11|f	1.48
3,3	30.9|442|590	200|173|420|150|140(□)	424|B+D,hook	510|y+s	1.13|f	1.46
3,4	32.6|474|638	200|154|420|150|140(□)	402|C,hook	435|y+s	1.07|f	1.57
1A,1	26.6|493|580	300|270|420|180|140(□)	766|B,hook	1150|s	1.33|s	0.71
1A,2	36.8|505|566	300|270|420|180|140(□)	755|D,hook	900|s	0.89|s	0.82
1A,2 bis	33.3|505|566	300|270|420|180|140(□)	755|D,hook	1178|s	1.22|s	0.79
1A,3	36.6|508|584	300|270|420|180|140(□)	656|B+D,hook	1185|s	1.22|s	0.86
1A,4	32.9|497|567	300|270|420|180|140(□)	766|C,hook	1158|s	1.21|s	0.78
3A,1	29.2|506|580	200|170|420|180|140(□)	766|B,hook	815|s	1.07|f	1.08
3A,2	39.2|505|582	200|170|420|180|140(□)	755|D,hook	900|s	1.14|f	1.20
3A,3	32.0|499|572	200|172|420|180|140(□)	656|B+D,hook	665|s	0.97|f	1.21
3A,3bis	46.1|499|572	200|172|420|180|140(□)	656|B+D,hook	843|f	1.18|f	1.37
3A,4	32.4|493|572	200|170|420|180|140(□)	766|C,hook	845|s	1.11|f	1.14
Q,1	33.9|460|608	200|170|420|150|140(□)	403|G,hook	408|f	0.93|f	1.29
Q,2	30.8|342|442	300|272|420|150|140(□)	628|G,hook	650|y+s	0.93|y+s	0.89
Q,2bis	21.0|325|464	300|273|420|150|140(□)	806|G,hook	510|y+s	0.81|s	0.65
6,1	13.2|498|592	140|107|420|150|140(□)	628|B,hook	250|s	1.05|s	0.80
6,2	13.2|461|535	140|106|420|150|140(□)	1232|B,hook	290|s	1.07|s	0.63
6,3	22.1|512|593	200|180|420|150|140(□)	628|B,hook	650|f	1.04|f	1.01
6,4	30.6|476|558	200|171|420|150|140(□)	1232|B,hook	850|s	0.97|s	0.88
6,5	18.4|518|618	300|264|420|150|140(□)	905|B,hook	842|s	1.22|s	0.55
6,6	18.4|468|555	300|280|420|150|140(□)	1608|B,hook	810|s	1.09|s	0.39
9A,1	22.6|459|636	500|474|420|150|140(□)	904|B,hook	1200|s	1.05|s	0.48
9A,2	33.9|467|595	500|471|420|150|140(□)	1608|B,hook	1900|s	1.18|s	0.43
9A,3	28.6|465|616	500|474|420|150|140(□)	1809|B+G,hook	1700|s	1.26|s	0.32
10,1a	28.7|446|605	250|226|420|150|140(□)	904|B,hook	850|s	1.20|s	0.63
10,1b	35.8|468|593	250|221|420|150|140(□)	888|B+D,hook	800|s	1.01|s	0.72
10,2a	28.2|453|615	250|218|420|150|140(□)	904|B,hook	750|s	1.06|s	0.64
10,2b	26.1|471|592	250|220|420|150|140(□)	886|B+D,hook	800|s	1.19|s	0.65
10,3a	23.6|462|630	250|223|420|150|140(□)	904|B,hook	760|s	1.19|s	0.57
10,3b	27.7|472|601	250|215|420|150|140(□)	886|B+D,hook	740|s	1.06|s	0.67
11,1a	22.3|311|431	300|272|420|150|140(□)	904|B,hook	563|y+s	0.74|s	0.76
11,1b	16.2|311|431	300|272|420|150|140(□)	904|B,nil	493|y+s	0.80|s	0.65
11,2a	25.6|445|545	300|288|420|150|140(□)	628|B,hook	558|s	0.77|s	0.75
11,2b	24.9|441|546	300|275|420|150|140(□)	628|B,nil	585|y+s	0.80|s	0.79
12,1a	17.3|319|436	200|171|420|150|140(□)	904|B,hook	840|f	1.43|y+s	0.99
12,1b	18.2|319|436	200|171|420|150|140(□)	904|B,nil	693|f	1.16|f	1.02
12,2a	27.0|436|541	200|173|420|150|140(□)	628|B,hook	750|y+s	1.31|f	1.21
12,2b	21.7|432|543	200|170|420|150|140(□)	628|B,nil	640|y+s	1.17|f	1.13
Clarke[2]						
A1	21.3|410|590	450|400|600|200|200(●)	785 | G,hook	1110 | s	1.11 | y+s	0.77
A2	27.6|410|590	450|400|600|200|200(●)	785 | B,hook	1420 | s	1.08 | y+s	0.98
A3	30.8|410|590	450|400|600|200|200(●)	778 | D,hook	1340 | s	1.00 | f	1.03

A4	21.4|410|590	450|400|600|200|200(●)	785 | G,nil	1230 | s	1.23 | y+s	0.77
A5	27.7|410|590	450|400|600|200|200(●)	785 | B,nil	1400 | s	1.06 | y+s	0.98
A6	26.9|410|590	450|400|600|200|200(●)	778 | D,nil	1230 | s	0.95 | y+s	0.98
A7	25.2|410|590	450|400|600|200|200(●)	785 | G,full	1640 | s	1.30 | y+s	0.95
A8	27.6|410|590	450|400|600|200|200(●)	785 | B,hook	1510 | s	1.15 | y+s	0.98
A9	27.7|410|590	450|400|600|200|200(●)	785 | G,hook	1450 | s	1.29 | y+s	0.84
A10	18.8|410|590	450|400|600|200|200(●)	785 | G,full+bob	1520 | f	1.40 | y+s	0.85
A11	18.0|410|590	450|400|600|200|200(●)	785 | G,full	1640 | f	1.55 | y+s	0.83
A12	26.3|410|590	450|400|600|200|200(●)	785 | G,full+bob	1640 | f	1.28 | y+s	0.96
B1	27.8|410|590	450|400|400|200|200(●)	628 | G,full	2080 | s	1.25 | y+s	0.97
B3	34.0|410|590	450|400|400|200|200(●)	471 | G,full	1770 | f	1.27 | f	1.20
Suzuki et al.[8]						
BP-20-1	21.3|413|606	200|150|540|300|150(●)	570 | G,hook	519 | y+s	1.19 | y+s	0.84
BP-20-2	20.4|413|606	200|150|540|300|150(●)	570 | G,hook	480 | y+s	1.12 | y+s	0.83
BPC-20-1	21.9|413|606	200|150|540|300|150(●)	570 | B,hook	519 | y+s	1.01 | y+s	0.98
BPC-20-2	19.9|413|606	200|150|540|300|150(●)	570 | B,hook	529 | y+s	1.07 | y+s	0.96
BP-25-1	22.6|413|606	250|200|540|300|150(●)	713 | G,hook	735 | s	1.14 | y+s	0.76
BP-25-2	21.5|413|606	250|200|540|300|150(●)	713 | G,hook	755 | s	1.19 | y+s	0.74
BPC-25-1	18.9|413|606	250|200|540|300|150(●)	713 | B,hook	818 | y+s	1.19 | y+s	0.83
BPC-25-2	22.0|413|606	250|200|540|300|150(●)	713 | B,hook	813 | y+s	1.09 | y+s	0.88
BP-20-30-1	29.1|405|592	200|150|500|300|150(●)	428 | G,hook	485 | y+s	1.01 | f	1.10
BP-20-30-2	29.8|405|592	200|150|500|300|150(●)	428 | G,hook	480 | y+s	1.00 | f	1.10
BPC-20-30-1	29.8|405|592	200|150|500|300|150(●)	428 | B,hook	500 | f	1.04 | f	1.29
BPC-20-30-2	29.8|405|592	200|150|500|300|150(●)	428 | B,hook	495 | f	1.03 | f	1.29
BP-30-30-1	27.3|405|592	300|250|500|300|150(●)	570 | G,hook	916 | s	1.18 | y+s	0.76
BP-30-30-2	28.5|405|592	300|250|500|300|150(●)	570 | G,hook	907 | y+s	1.15 | y+s	0.77
BPC-30-30-1	28.9|405|592	300|250|500|300|150(●)	570 | B,hook	1039 | y+s	1.12 | y+s	0.90
BPC-30-30-2	30.9|405|592	300|250|500|300|150(●)	570 | B,hook	1029 | y+s	1.08 | y+s	0.92
BP-30-25-1	30.9|405|592	300|250|500|250|150(●)	570 | G,hook	794 | y+s	1.09 | y+s	0.82
BP-30-25-2	26.3|405|592	300|250|500|250|150(●)	570 | G,hook	725 | s	1.07 | y+s	0.77
BPC-30-25-1	29.1|405|592	300|250|500|250|150(●)	570 | B,hook	853 | y+s	1.02 | y+s	0.94
BPC-30-25-2	29.2|405|592	300|250|500|250|150(●)	570 | B,hook	872 | y+s	1.04 | y+s	0.94
BDA-70x90-1	29.1|356|501	300|250|500|250|150(●)	570 | G,hook	784 | y+s	1.02 | y+s	0.99
BDA-70x90-2	30.2|356|501	300|250|500|250|150(●)	570 | G,hook	755 | y+s	0.97 | f	1.01
BDA-80x90-1	29.1|356|501	300|250|500|250|150(●)	570 | G,hook	858 | y+s	1.11 | f	1.02
BDA-80x90-2	29.3|356|501	300|250|500|250|150(●)	570 | G,hook	853 | y+s	1.10 | f	1.02
BDA-90x90-1	29.5|356|501	300|250|500|250|150(●)	570 | G,hook	853 | y+s	1.10 | f	1.05
BDA-90x90-2	31.5|356|501	300|250|500|250|150(●)	570 | G,hook	921 | y+s	1.18 | f	1.07
BDA-100x90-1	29.7|356|501	300|250|500|250|150(●)	570 | G,hook	911 | y+s	1.17 | f	1.08
BDA-100x90-2	31.3|356|501	300|250|500|250|150(●)	570 | G,hook	931 | y+s	1.19 | f	1.10
Suzuki et al.[9]						
TDL1-1	30.9|356|501	350|300|600|250|150(●)	285 | G,hook	392 | f	0.99 | f	1.30
TDL1-2	28.2|356|501	350|300|600|250|150(●)	285 | G,hook	392 | f	0.99 | f	1.25
TDL2-1	28.6|356|501	350|300|600|250|150(●)	428 | G,hook	519 | f	0.91 | f	1.02
TDL2-2	28.8|356|501	350|300|600|250|150(●)	428 | G,hook	472 | f	0.83 | f	1.02
TDL3-1	29.6|356|501	350|300|600|250|150(●)	570 | G,hook	608 | f	0.93 | y+s	0.89
TDL3-2	29.3|356|501	350|300|600|250|150(●)	570 | G,hook	627 | f	0.96 | y+s	0.89
TDS1-1	25.6|356|501	350|300|450|250|150(●)	428 | G,hook	921 | f	1.15 | y+s	0.97
TDS1-2	27.0|356|501	350|300|450|250|150(●)	428 | G,hook	833 | f	1.02 | y+s	0.97
TDS2-1	27.2|356|501	350|300|450|250|150(●)	570 | G,hook	1005 | f	1.12 | y+s	0.85
TDS2-2	27.3|356|501	350|300|450|250|150(●)	570 | G,hook	1054 | f	1.17 | y+s	0.85
TDS3-1	28.0|356|501	350|300|450|250|150(●)	784 | G,hook	1299 | y+s	1.29 | s	0.73
TDS3-2	28.1|356|501	350|300|450|250|150(●)	784 | G,hook	1303 | y+s	1.29 | s	0.73
TDM1-1	27.5|383|522	300|250|500|250|150(●)	285 | G,hook	490 | f	1.11 | f	1.25
TDM1-2	26.3|383|522	300|250|500|250|150(●)	285 | G,hook	461 | f	1.05 | f	1.23
TDM2-1	29.6|383|522	300|250|500|250|150(●)	428 | G,hook	657 | f	1.04 | f	1.04
TDM2-2	27.6|383|522	300|250|500|250|150(●)	428 | G,hook	657 | f	1.05 | f	1.01
TDM3-1	27.0|370|528	300|250|500|250|150(●)	1270 | G,hook	1245 | s	1.42 | s	0.57
TDM3-2	28.0|370|528	300|250|500|250|150(●)	1270 | G,hook	1210 | s	1.36 | s	0.58
Suzuki et al.[10]						
BDA-20-25-70-1	26.1|358|496	200|150|450|250|150(●)	285 | G,hook	294 | f	1.00 | f	1.54

BDA-20-25-70-2	26.1|358|496	200|150|450|250|150(●)	285 | G,hook	304 | f	1.03 | f	1.54
BDA-20-25-80-1	25.4|358|496	200|150|450|250|150(●)	285 | G,hook	304 | f	1.04 | f	1.51
BDA-20-25-80-2	25.4|358|496	200|150|450|250|150(●)	285 | G,hook	304 | f	1.04 | f	1.51
BDA-20-25-90-1	25.8|358|496	200|150|450|250|150(●)	285 | G,hook	333 | f	1.13 | f	1.53
BDA-20-25-90-2	25.8|358|496	200|150|450|250|150(●)	285 | G,hook	333 | f	1.13 | f	1.53
BDA-30-20-70-1	25.2|358|496	300|250|450|200|150(●)	428 | G,hook	534 | f	0.90 | f	1.05
BDA-30-20-70-2	24.6|358|496	300|250|450|200|150(●)	428 | G,hook	549 | y+s	0.93 | f	1.05
BDA-30-20-80-1	25.2|358|496	300|250|450|200|150(●)	428 | G,hook	568 | f	0.96 | f	1.05
BDA-30-20-80-2	26.6|358|496	300|250|450|200|150(●)	428 | G,hook	564 | f	0.94 | f	1.08
BDA-30-20-90-1	26.0|358|496	300|250|450|200|150(●)	428 | G,hook	583 | f	0.98 | f	1.06
BDA-30-20-90-2	26.1|358|496	300|250|450|200|150(●)	428 | G,hook	588 | f	0.99 | f	1.06
BDA-30-25-70-1	28.8|383|522	300|250|450|250|150(●)	428 | G,hook	662 | y+s	0.91 | f	1.02
BDA-30-25-70-2	26.5|383|522	300|250|450|250|150(●)	428 | G,hook	676 | y+s	0.95 | y+s	0.99
BDA-30-25-80-1	29.4|383|522	300|250|450|250|150(●)	428 | G,hook	696 | y+s	0.95 | f	1.02
BDA-30-25-80-2	27.8|383|522	300|250|450|250|150(●)	428 | G,hook	725 | y+s	1.00 | f	1.00
BDA-30-25-90-1	29.0|383|522	300|250|450|250|150(●)	428 | G,hook	764 | y+s	1.05 | f	1.03
BDA-30-25-90-2	26.8|383|522	300|250|450|250|150(●)	428 | G,hook	764 | f	1.06 | y+s	0.99
BDA-30-30-70-1	26.8|358|496	300|250|450|300|150(●)	428 | G,hook	769 | y+s	0.94 | y+s	0.99
BDA-30-30-70-2	25.9|358|496	300|250|450|300|150(●)	428 | G,hook	730 | y+s	0.91 | y+s	0.98
BDA-30-30-80-1	27.4|358|496	300|250|450|300|150(●)	428 | G,hook	828 | y+s	1.01 | y+s	1.00
BDA-30-30-80-2	27.4|358|496	300|250|450|300|150(●)	428 | G,hook	809 | y+s	0.98 | y+s	1.00
BDA-30-30-90-1	27.2|358|496	300|250|450|300|150(●)	428 | G,hook	843 | y+s	1.03 | y+s	0.99
BDA-30-30-90-2	24.5|358|496	300|250|450|300|150(●)	428 | G,hook	813 | y+s	1.05 | y+s	0.96
BDA-40-25-70-1	25.9|358|496	400|350|450|250|150(●)	570 | G,hook	1019 | s	1.06 | y+s	0.80
BDA-40-25-70-2	24.8|358|496	400|350|450|250|150(●)	570 | G,hook	1068 | y+s	1.13 | y+s	0.78
BDA-40-25-80-1	26.5|358|496	400|350|450|250|150(●)	570 | G,hook	1117 | f	1.15 | y+s	0.80
BDA-40-25-80-1	25.5|358|496	400|350|450|250|150(●)	570 | G,hook	1117 | y+s	1.17 | y+s	0.79
BDA-40-25-90-1	25.7|358|496	400|350|450|250|150(●)	570 | G,hook	1176 | f	1.23 | y+s	0.79
BDA-40-25-90-2	26.0|358|496	400|350|450|250|150(●)	570 | G,hook	1181 | f	1.23 | y+s	0.80
Suzuki et al.[11]						
BPL-35-30-1	24.1|353|505	350|300|500|300|150(●)	642 | G,hook	960 | s	1.11 | y+s	0.75
BPL-35-30-2	25.6|353|505	350|300|500|300|150(●)	642 | G,hook	941 | s	1.06 | y+s	0.76
BPB-35-30-1	23.7|353|505	350|300|500|300|150(●)	642 | G,full+bob	1029 | y+s	1.04 | y+s	0.86
BPB-35-30-2	23.5|353|505	350|300|500|300|150(●)	642 | G,full+bob	1103 | y+s	1.12 | y+s	0.85
BPH-35-30-1	31.5|353|505	350|300|500|300|150(●)	642 | G,hook	980 | s	1.00 | y+s	0.82
BPH-35-30-2	32.7|353|505	350|300|500|300|150(●)	642 | G,hook	1088 | y+s	1.09 | y+s	0.83
BPL-35-25-1	27.1|353|505	350|300|500|250|150(●)	642 | G,hook	902 | y+s	1.09 | y+s	0.81
BPL-35-25-2	25.6|353|505	350|300|500|250|150(●)	642 | G,hook	872 | s	1.08 | y+s	0.79
BPB-35-25-1	23.2|353|505	350|300|500|250|150(●)	642 | G,full+bob	911 | y+s	1.02 | y+s	0.89
BPB-35-25-2	23.7|353|505	350|300|500|250|150(●)	642 | G,full+bob	921 | y+s	1.02 | y+s	0.89
BPH-35-25-1	36.6|353|505	350|300|500|250|150(●)	642 | G,hook	882 | s	0.94 | y+s	0.89
BPH-35-25-2	37.9|353|505	350|300|500|250|150(●)	642 | G,hook	951 | s	0.99 | y+s	0.90
BPL-35-20-1	22.5|353|505	350|300|500|200|150(●)	642 | G,hook	755 | s	1.09 | y+s	0.78
BPL-35-20-2	21.5|353|505	350|300|500|200|150(●)	642 | G,hook	735 | s	1.08 | y+s	0.77
BPB-35-20-1	20.4|353|505	350|300|500|200|150(●)	642 | G,full+bob	755 | y+s	0.99 | y+s	0.87
BPB-35-20-2	20.2|353|505	350|300|500|200|150(●)	642 | G,full+bob	804 | y+s	1.06 | y+s	0.86
BPH-35-20-1	31.4|353|505	350|300|500|200|150(●)	642 | G,hook	813 | s	1.02 | y+s	0.87
BPH-35-20-2	30.8|353|505	350|300|500|200|150(●)	642 | G,hook	794 | s	1.00 | y+s	0.86
Chan and Poh[21]						
A	39.7|481|601	400|325|600|200|150(●)	628 | G,full	1230 | f	1.31 | f	1.11
B	38.3|481|601	400|325|600|200|150(●)	628 | G,full	1250 | f	1.34 | f	1.10
C	36.4|481|601	300|225|600|200|150(●)	942 | G,full	870 | y+s	0.97 | f	1.05

Note: □ = square pile; ● = circular pile; B = square bunched reinforcement; D = diagonal bunched reinforcement; G = grid reinforcement; C = continuous bunched reinforcement; f = flexural failure; s = shear failure; y+s = reinforcement yielding followed by shear failure; 1 mm = 0.04 in.; 1 mm^2 = 0.0015 in.^{2}; 1 MPa = 145 psi; 1 kN = 0.225 kip

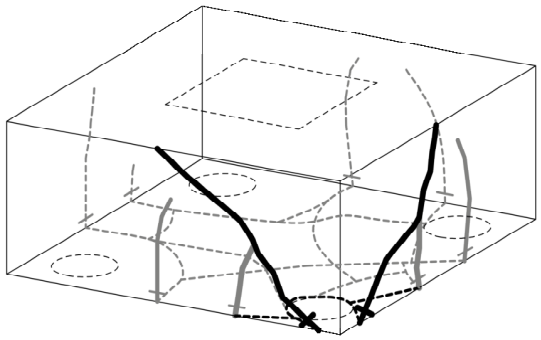

Fig. 1– Punching failure around pile (after reference[8]).

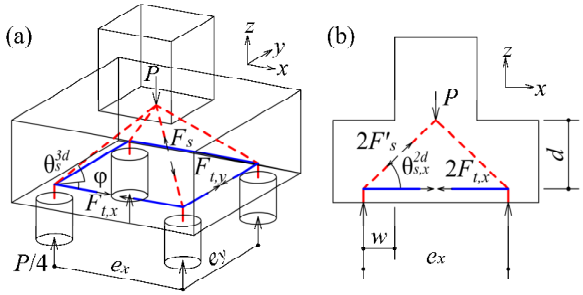

Fig. 2– Strut-and-tie models for four-pile cap without shear reinforcement (a) 3D, (b) 2D.

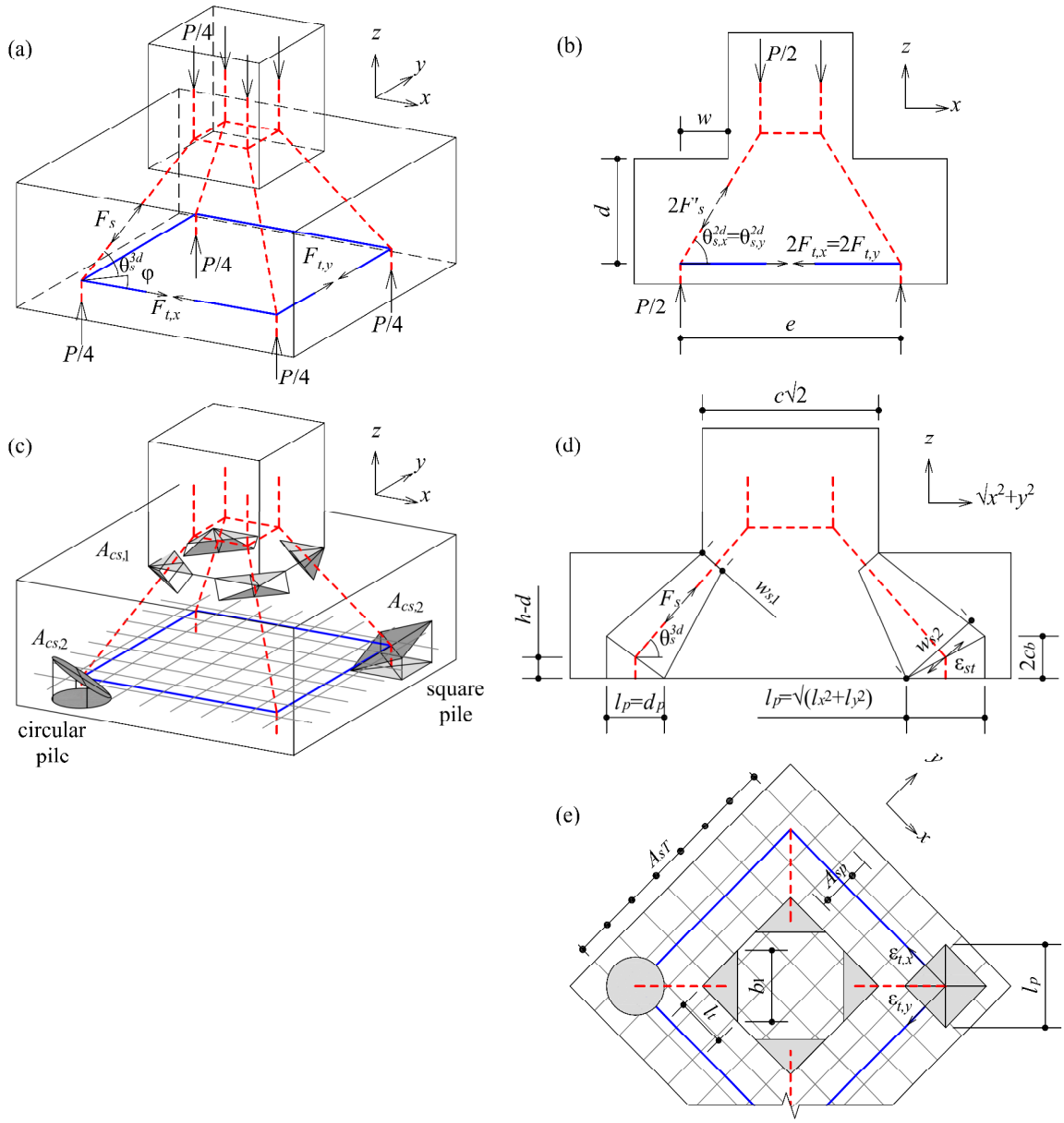

Fig. 3– Proposed strut-and-tie model: (a) 3D truss; (b) 2D truss; (c) 3D view of strut and tie details, (d) strut projection onto cap diagonal plane and (e) plan view of strut and tie details.

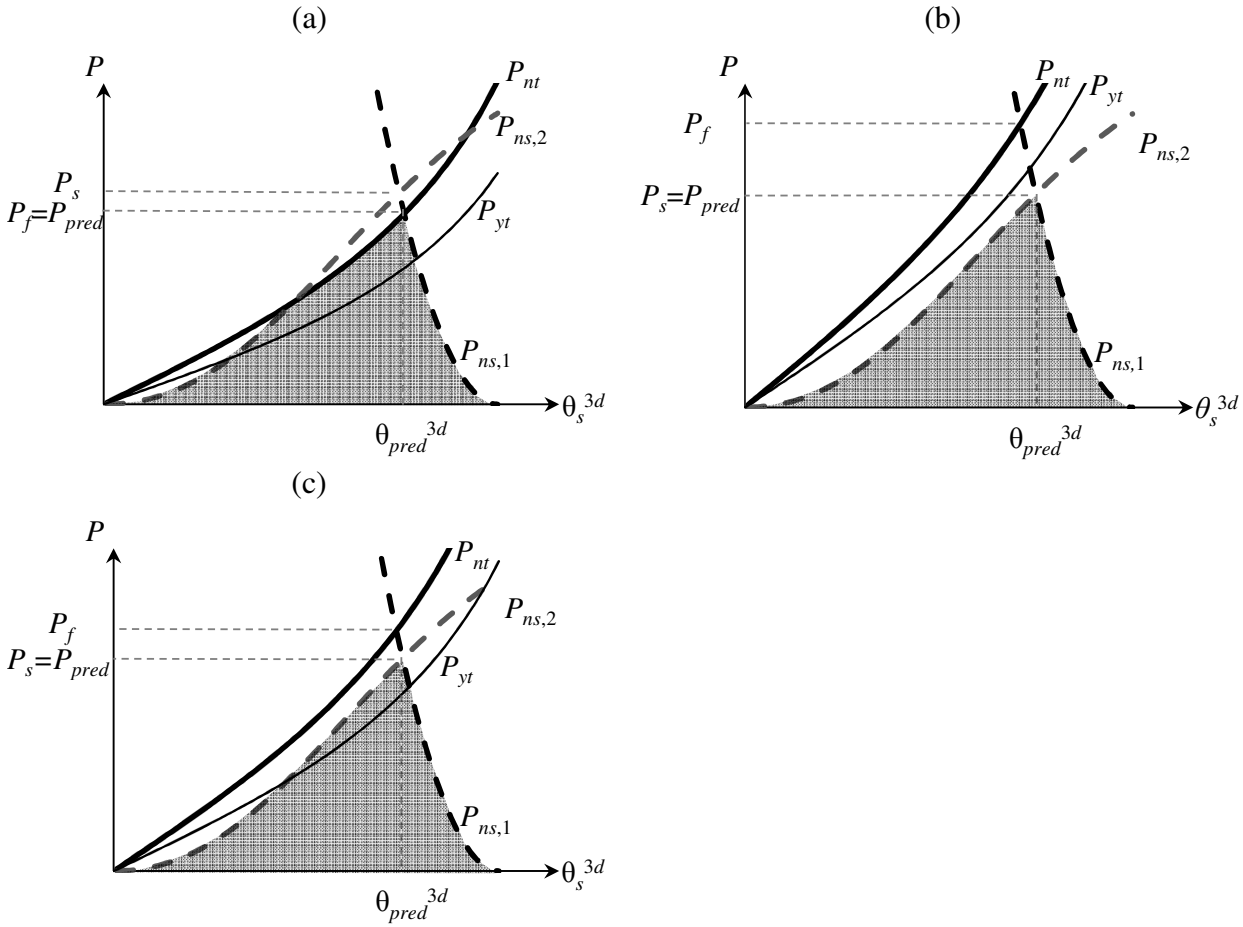

Fig. 4 – Limit functions P_{nt}, $P_{ns,1}$ and $P_{ns,2}$ and yielding function P_{yt} to predict pile cap strength: (a) flexural failure, (b) shear failure prior reinforcement yielding and (c) shear failure after reinforcement yielding.

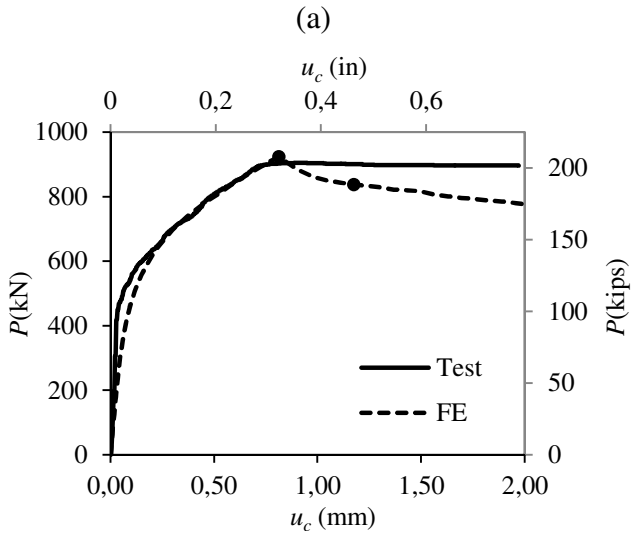

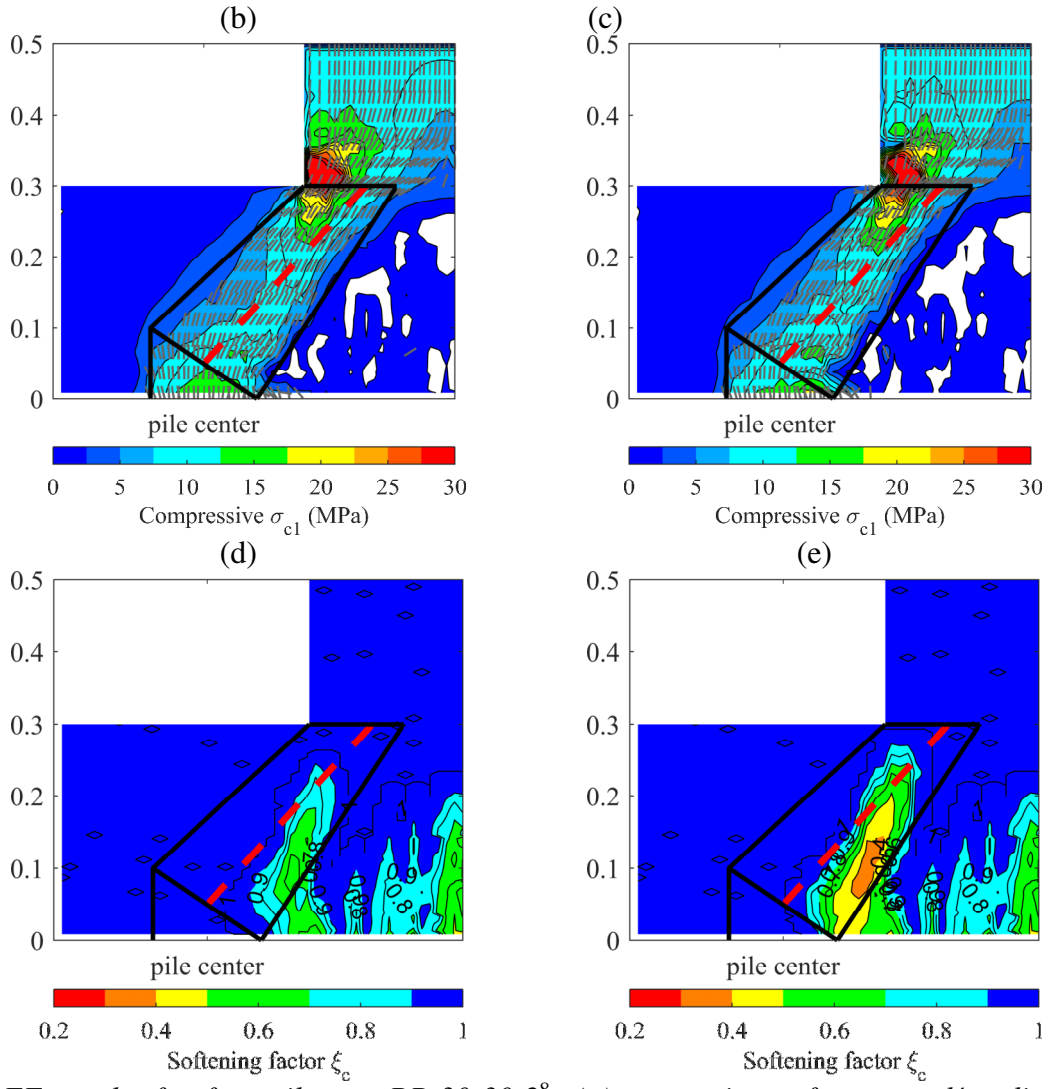

Fig. 5 – FE results for four-pile cap BP-30-30-2[8]*: (a) comparison of measured/predicted load-deflection curve. At the diagonal cap plane, superimposed to the strut-and-tie geometry obtained from the proposed method (θ_s^{3d} =48.64º): (b) FE contour plot of compressive stress field and principal compressive directions at maximum load; (c) FE contour plot of compressive stress field and principal compressive directions after failure; (d) FE contour plot of concrete softening coefficient ξ at maximum load; (e) contour plot of concrete softening coefficient ξ after failure.*

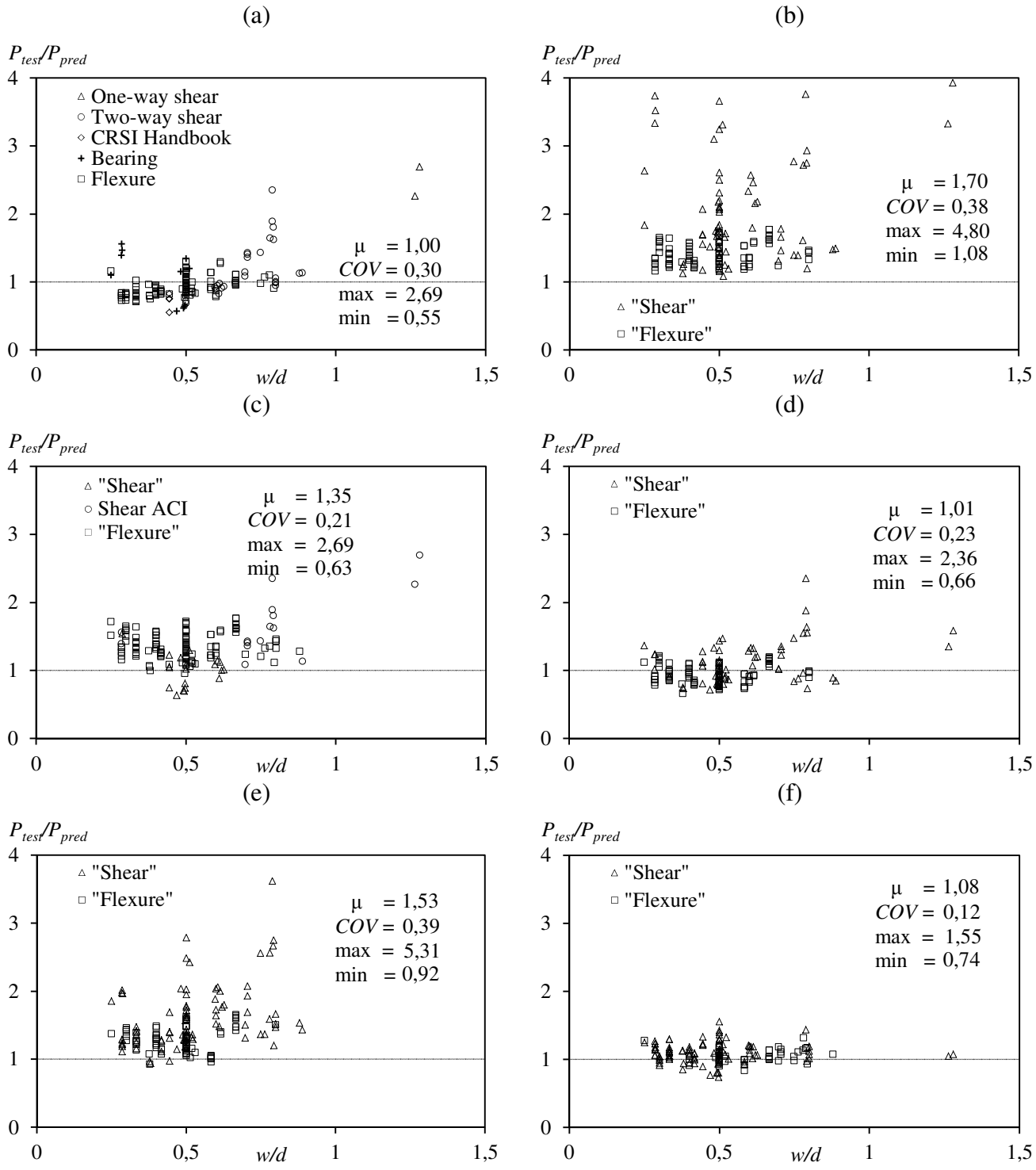

Fig. 6 - Ratio P_{test} / P_{pred} for 162 specimens[1,2,8,9,10,11,25] *based on results obtained by: (a) ACI sectional approach*[12]*, (b)ACI STM*[12] *(c) Adebar and Zhou*[4]*, (d) Souza et al.*[6] *(e) Park et al.*[5] *and (f) the proposed method.*

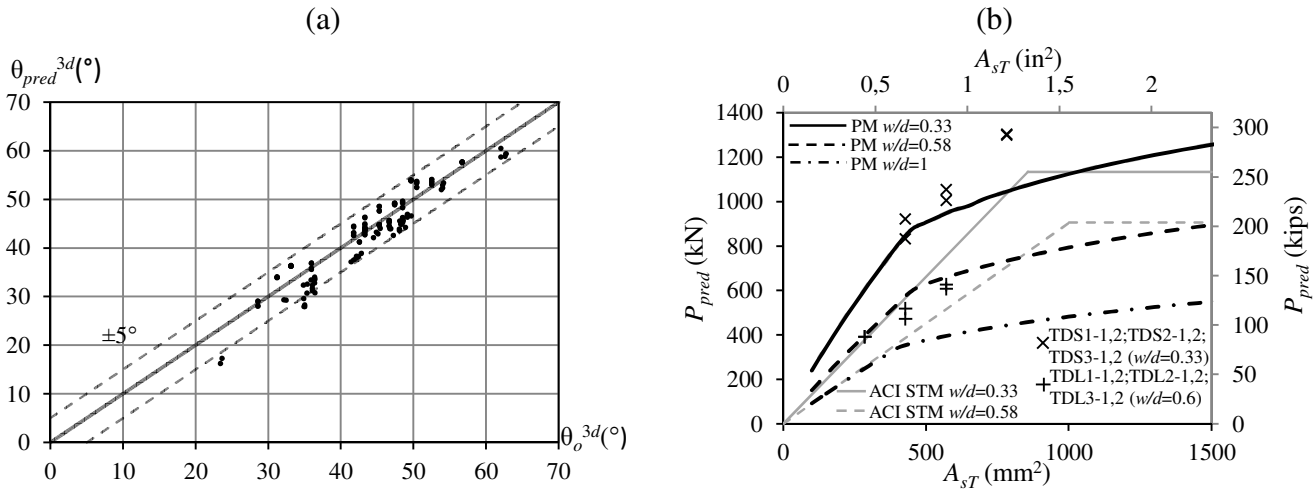

Fig. 7 –(a) Fixed strut angle θ_o^{3d} adopted by other truss models vs. predicted strut angle at failure θ_{pred}^{3d} by the proposed model for 162 specimens[1,2,8,9,10,11,25]*; (b) Effect of reinforcement quantity A_{sT} for different values of w/d on predicted strength by proposed model (PM).*

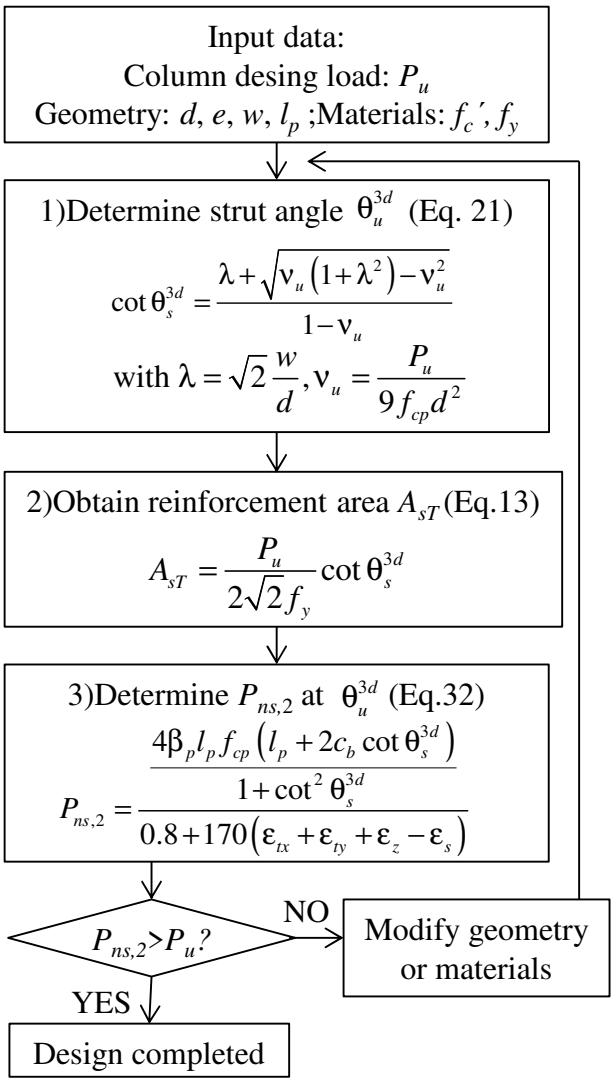

Fig. 8 –Flowchart of proposed design method.